


## Article

# Tensile Characteristics and Fracture Mode of Frozen Fractured Rock Mass Based on Brazilian Splitting Test

Tingting Wang <sup>1</sup> , Pingfeng Li <sup>2,\*</sup>, Chun'an Tang <sup>3,4</sup>, Bingbing Zhang <sup>2</sup>, Jiang Yu <sup>1</sup> and Tao Geng <sup>5</sup><sup>1</sup> School of Resources and Civil Engineering, Northeastern University, Shenyang 110819, China<sup>2</sup> Hongda Blasting Engineering Group Co., Ltd., Guangzhou 510623, China<sup>3</sup> State Key Laboratory of Coastal and Offshore Engineering, Dalian University of Technology, Dalian 116024, China<sup>4</sup> State Key Laboratory of Frozen Soil Engineering, Northwest Institute of Eco-Environment and Resources, Chinese Academy of Sciences, Lanzhou 730000, China<sup>5</sup> School of Earth Sciences, China University of Geosciences, Wuhan 430074, China

\* Correspondence: hdbplpf@163.com

**Abstract:** Frozen fractured rock mass is often encountered during the implementation of geotechnical engineering in cold regions. The tensile strength parameters of frozen rock play an important role in the construction of rock slopes involving tensile failure. In order to study the tensile characteristics of a frozen fractured rock mass in a cold region, original rock specimens were mined and processed in the Yulong Copper Mine, and artificial, frozen fractured marble specimens were made. The effects of different ice-filled crack angles, lengths, and widths on the force–displacement curve and the tensile strength of frozen rock were studied by laboratory Brazilian splitting experiments and RFPA<sup>3D</sup>, and the evolution law of the tensile strength of frozen rock was revealed. At the same time, wing crack initiation and cracking mode after tensile failure were analyzed by high-speed camera; the whole process of the Brazilian splitting of frozen rock was reconstructed, and the development of microcrack initiation in frozen rock was analyzed. The following conclusions were drawn from the test results: the frozen rock specimens have typical brittle-failure characteristics. The tensile strength of frozen rock decreases gradually with the increase in the width and length of ice-filled cracks, and decreases first and then increases with the increase in the angle of the ice-filled crack. The ice-filled crack incurs damage first, and then the wing cracks start from the tip of the ice-filled crack and extend continuously. The tensile strength of frozen rock is significantly affected by the angle and length of ice-filled cracks.

**Keywords:** frozen rock mass; Brazilian splitting test; tensile strength; ice-filled crack ice; failure characteristics



**Citation:** Wang, T.; Li, P.; Tang, C.; Zhang, B.; Yu, J.; Geng, T. Tensile Characteristics and Fracture Mode of Frozen Fractured Rock Mass Based on Brazilian Splitting Test. *Appl. Sci.* **2022**, *12*, 11788. <https://doi.org/10.3390/app122211788>

Academic Editor: Arcady Dyskin

Received: 20 October 2022

Accepted: 18 November 2022

Published: 20 November 2022

**Publisher's Note:** MDPI stays neutral with regard to jurisdictional claims in published maps and institutional affiliations.



**Copyright:** © 2022 by the authors. Licensee MDPI, Basel, Switzerland. This article is an open access article distributed under the terms and conditions of the Creative Commons Attribution (CC BY) license (<https://creativecommons.org/licenses/by/4.0/>).

## 1. Introduction

The Yulong Copper Mine in Tibet, China, is 4569–5118 m above sea level. The mining area is a semi-arid alpine region with a continental climate, and has rich and reliable copper resources. This region mainly adopts a strip mining method. In the process of resource development, the rock slope of the strip mine in such high-altitude and cold regions is exposed for a long time, and there are cracks, weak interlayers, stratification, and other structural surfaces (Figure 1). Under rainfall and groundwater conditions, the fissures will gather water to form a frozen rock mass. In the process of mineral resource development, a frozen rock mass is often encountered. In order to carry out safe and efficient engineering and mining, a deep understanding of the mechanical properties of frozen rock mass is of crucial guiding significance for improving the development efficiency of open-pit mineral resources and construction safety and prevention of accidents in high altitude cold regions [1–7].

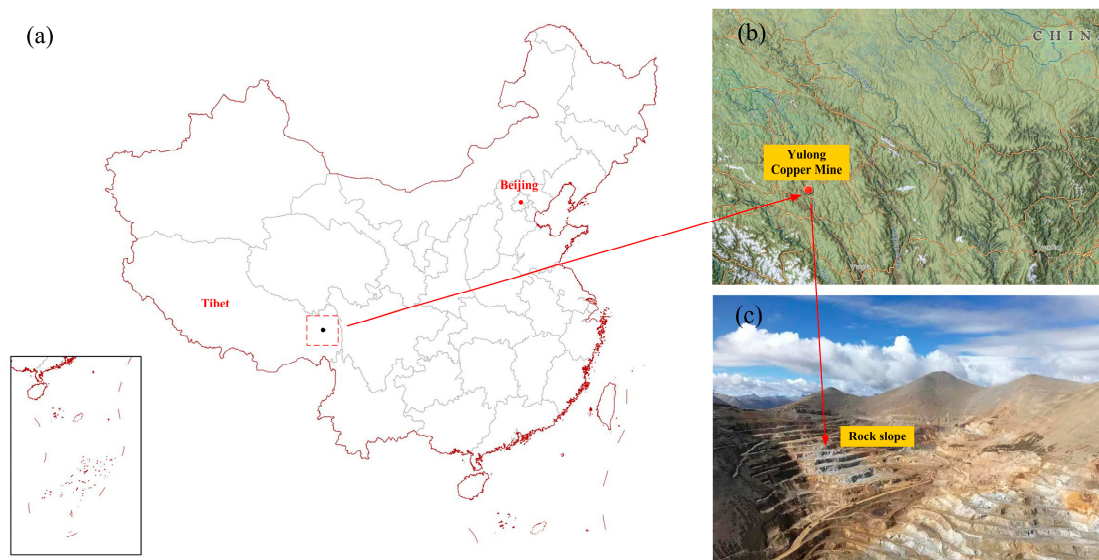


**Figure 1.** Yulong Copper Mine in Tibet, China. (a) Tibet Autonomous Region in Southwest China; (b) Satellite imagery of Yulong copper mine; (c) Rock slope in Yulong copper mine.

The tensile strength, compressive strength and shear strength of rock are important indicators for measuring the physical and mechanical properties of rock. The damage and failure of rock are usually controlled by the tensile strength. There are two main methods to test the tensile strength of rock, the first is direct stretching, and the second is indirect stretching. However, the direct tensile test requires specific laboratory equipment and complex operations, and the indirect tensile test has a more mature theoretical system. So, the indirect tensile test, namely the Brazilian splitting test, is generally used to test the tensile strength of rock [8,9].

Many scholars [10–13] have analyzed the changes of tensile strength, tensile sensitivity coefficient, radial strain, AE energy accumulation and release, crack initiation and fracture mode of rock specimens through the Brazilian splitting laboratory test and numerical simulation. Their research considered the prefabricated fissures, pores, different strain rates, degrees of water saturation, different particle sizes, different angles, high temperatures, filling of fissures, and other factors. At present, there are mature theoretical systems and methods for reference. The research on low-temperature rock mechanics mainly focuses on the mechanical properties of frozen intact rock [14–17] and the influence of the freeze–thaw cycle on the failure characteristics of the rock’s mechanical properties [18–21]. The mechanical properties of frozen intact rock are mainly determined by freezing temperature, initial water content and loading rate. Aoki et al. [22] studied the mechanical properties of various rocks under dry or saturated conditions through uniaxial compression and Brazilian splitting tests. The results showed that the compressive and tensile strength and elastic modulus increased significantly at  $-160\text{ }^{\circ}\text{C}$ , and the compressive and tensile strength and elastic modulus varied according to the type of rock and the degree of water saturation. Yamabe et al. [23] studied the mechanical properties of sandstone at low temperatures through uniaxial and triaxial experiments. They found that the tensile and compressive strength of rock increased with the decrease in temperature. Still, the elastic modulus was less affected by temperature in the section from  $-10$  to  $-20\text{ }^{\circ}\text{C}$ . Xu et al., Yang et al., Xi et al., and Shan et al. [24–27] studied the mechanical properties of a variety of rocks under negative temperature through uniaxial and triaxial experiments. The results showed that the compressive strength, internal friction angle, cohesion force and elastic modulus of the rocks all increased with the decrease in temperature. They attributed the increase in mechanical properties with decreasing temperature to the shrinkage of mineral particles at low temperatures, the increased strength of the ice itself, and the interaction of the frost swelling force with the rock. Li et al. [28] studied the strength characteristics of frozen

limestone sandstone in different confining pressures under cyclic loading and unloading, and found that the peak strength increased under low confining pressures, while the peak strength ‘weakened’ under high confining pressures.

Some scholars have conducted compression experiments on frozen rock specimens with cracks at low temperatures. Bai et al. [29] studied the strength, deformation and crack evolution characteristics of frozen red sandstone with two ice-filled defects under different temperatures and sealing pressures. Yang et al. [30] studied the influence of crack inclination angle, length, width, confining pressure and temperature on the mechanical properties of single and double crack rock mass under low-temperature conditions. They found that Poisson’s ratio and elastic modulus were less affected by confining pressure under low-temperature conditions, and rock mass strength increased with the decrease in temperature. The inclination angle had the most significant effect on the strength of rock mass, followed by length and temperature. The above studies used red sandstones or similar materials to discuss the fracture mode and mechanical properties of frozen rock mass after compression. They considered the relevant engineering problems in the construction process of the artificial freezing method. The mechanical properties of the frozen fracture rock mass with high density which is encountered in the blasting construction of the cold region strip mine are not clear.

Currently, relevant studies on frozen fracture rock mass mainly evaluate the compressive strength. In contrast, field sampling in cold regions and tensile strength tests of frozen fracture rock mass have not been involved. In particular, there has not been a comprehensive and systematic analysis of the influence of ice-filled crack space distribution on the tensile strength of frozen fracture rock mass and the failure process of wing crack propagation under load. At the same time, it is difficult to obtain the original rock in a high altitude cold region project. So, it would be of great value to find an effective numerical simulation method to analyze the mechanical properties of frozen rock mass.

This study focused on the tensile strength of frozen fractured rock mass in high altitude cold regions. The aim of the study was to reveal the tensile characteristics and fracture mode of frozen fractured rock mass during the Brazilian splitting test process. The original rock sampling and processing were carried out from the Yulong Copper Mine in Tibet, China, to make artificial ice-filled crack marble specimens. The Brazilian splitting test of frozen rock mass was carried out. Firstly, the influence of ice-filled cracks with different angles on the strength and fracture mode of the frozen rock mass was investigated experimentally, and the initiation and propagation of wing cracks were recorded by a high-speed camera. Furthermore, the effects of the width and length of the ice-filled cracks on the tensile properties of rock mass were discussed by RFPA<sup>3D</sup>.

## 2. Test Preparation

### 2.1. Specimens Processing

All the marble rock specimens were taken from the Yulong Copper Mine in Tibet, China. The rock core was fabricated into a specimen, whose size was  $\phi = 50 \times 25$  mm. The selected specimens were processed through the carver to form different angled cracks (0, 30, 45, 60, 90°). Two of each specification were made for the post-production of ice-filled rock specimens. The test results and similar fracture modes were selected as the final test results to reduce the test error.

In order to prevent moisture migration during freezing and ensure uniform moisture in the specimen, the prepared specimens were first placed in a constant low temperature environment of  $-20$  °C for rapid freezing, and the freezing time was 48 h. Subsequently, a uniaxial compression testing machine was used as the power device to carry out the Brazilian splitting test on the frozen rock specimens (Figure 2). The constant deformation rate (0.001 mm/s) was loaded until the specimen was split. The tensile strength of the specimen was calculated using the formula proposed by Shluido [31]:

$$\sigma_t = \frac{2P}{\pi dt} \quad (1)$$

where  $\sigma_t$  is the failure load of the rock specimen,  $d$  is the diameter of the rock specimen, and  $t$  is the thickness of the rock specimen.

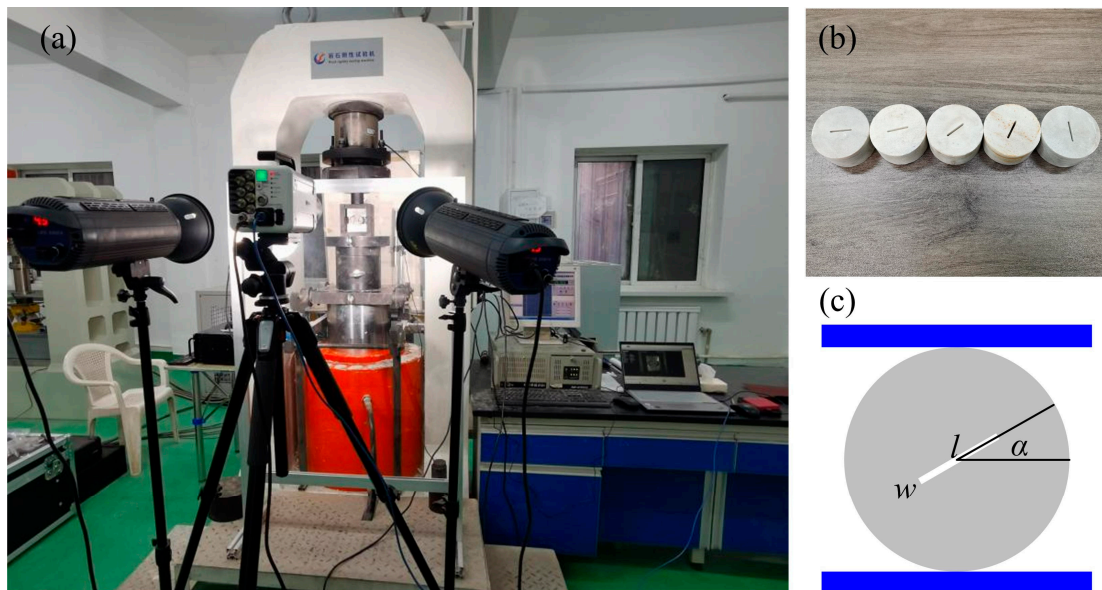


**Figure 2.** Design drawing of experimental device and specimen. (a) Photograph of experimental device; (b) Test specimens; (c)  $l$  is the ice-filled crack length,  $\alpha$  is the ice-filled crack angle, and  $w$  is the ice-filled crack width.

The compressive and tensile strengths of intact frozen rock under natural water were measured. The uniaxial compressive force–displacement curve of the frozen rock specimen fell sharply when it increased to 131.02 kN (Figure 3). When the tensile strength of the intact specimen reached the peak value of 8.88 kN, the stress curve fell quickly (Figure 4).

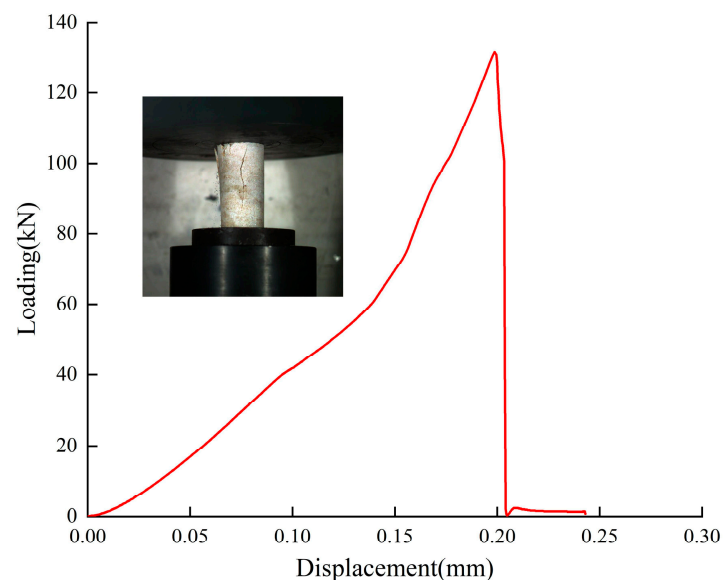


**Figure 3.** Uniaxial compression force–displacement curve of intact frozen rock specimen.



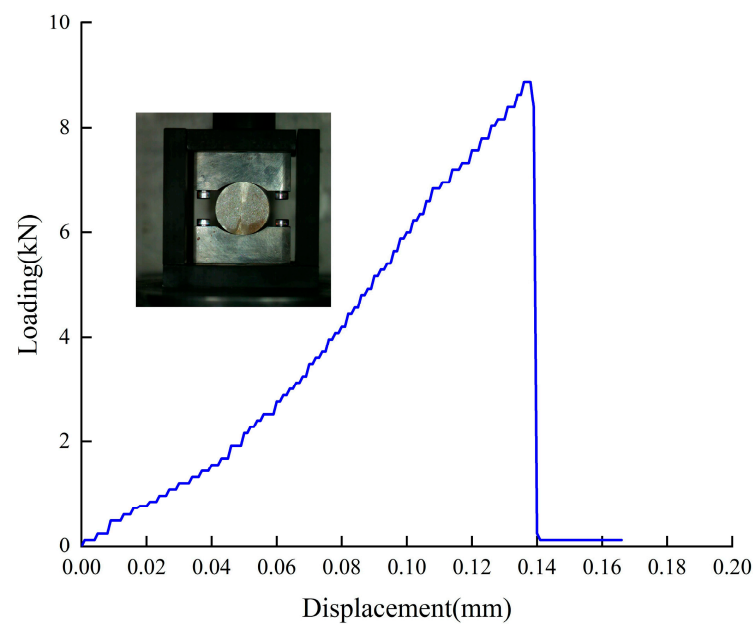


**Figure 4.** Brazilian splitting force–displacement curve of intact frozen rock specimen.

## 2.2. Test Results of Frozen Rock Specimens in Different Ice-Filled Crack Angles

### 2.2.1. Analysis of Tensile Strength

Figure 5 shows the Brazilian splitting force–displacement curve of frozen rock with different ice-filled crack angles. The study found that all the frozen rock specimens showed typical brittle failure characteristics. The tensile strength of the frozen rock specimens decreased gradually and then increased with the increase in the ice-filled crack angles. The tensile strength fell quickly after the peak, and the specimens fractured after producing a small displacement.

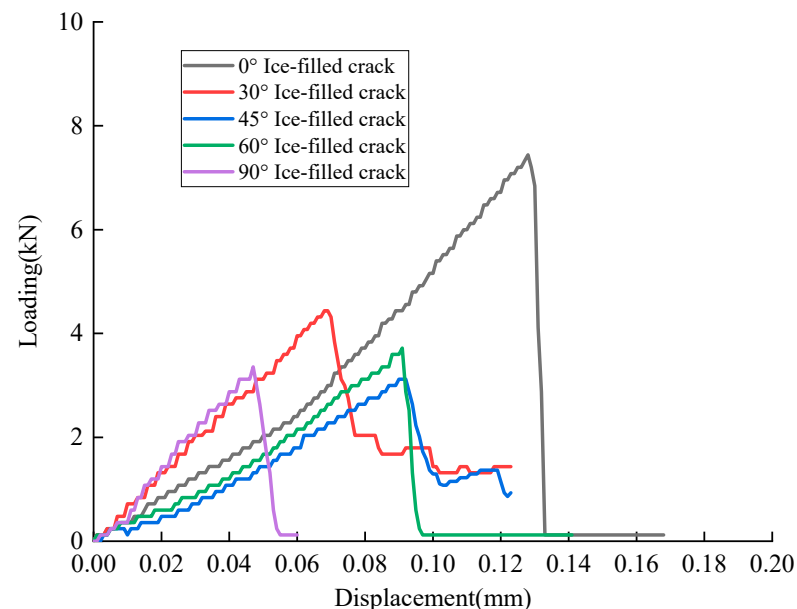


**Figure 5.** Brazilian splitting test force–displacement curve of frozen rocks with different ice-filled crack angles.

### 2.2.2. Analysis of Fracture Mode

Figures 6 and 7 show the splitting failure process of frozen rock specimens containing different ice-filled crack angles. The splitting failure is caused by the damage of ice during

loading, the wing crack penetration of the ice-filled crack tip and the extension of the far-field crack. In the process of splitting, the ice-filled crack incurs damage first, and then the wing crack at the tip extends to the top and bottom of the specimen, and the macroscopic crack is gradually formed. When the ice-filled crack angle  $\alpha$  is  $0^\circ$ , the ice-filled crack is perpendicular to the loading direction. The wing crack of the ice-filled crack tip cannot penetrate through the whole specimen along the ice-filled crack, and the tensile strength of the specimen is relatively high. When the ice-filled crack angle  $\alpha > 0^\circ$ , the ice crack's force bearing and transmission during loading gradually decrease with the increase in the ice-filled crack angle. Crack formation is hindered by the ice-filled crack. As the ice-filled crack angle  $\alpha$  increases, the crack evolution is less hindered. As the angle between the ice-filled crack and the loading direction gradually decreases, the crack and the ice-filled crack are quickly connected, eventually leading to specimen fracture. When the ice-filled crack angle  $\alpha$  is  $90^\circ$ , the ice-filled crack is parallel to the loading direction, and the fissure ice effect is minimized.

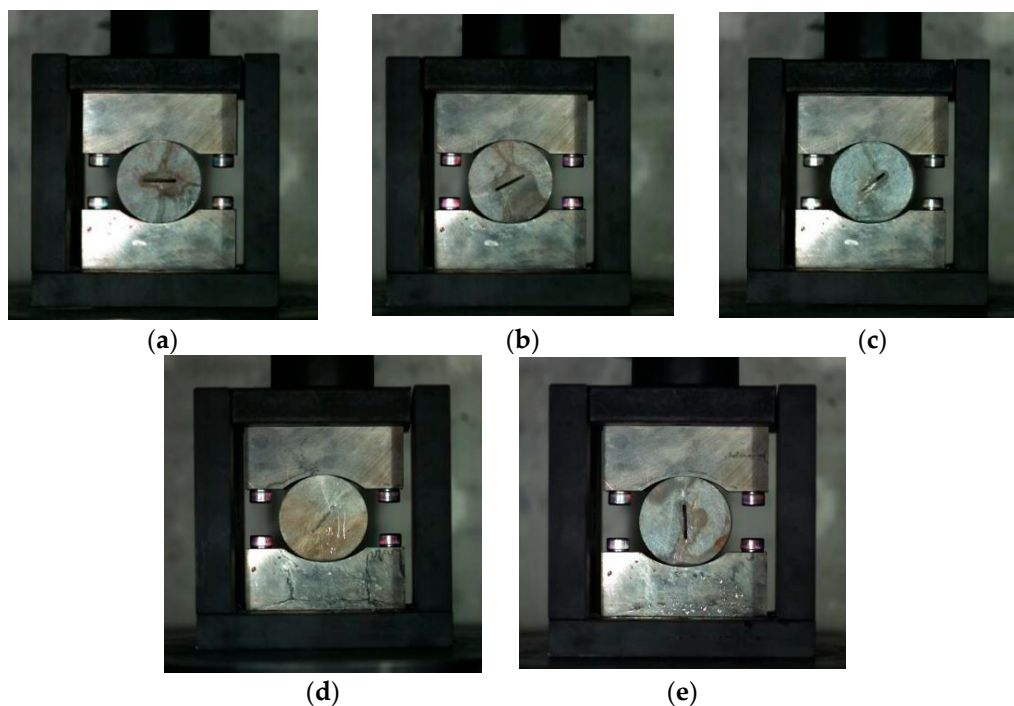


**Figure 6.** Fracture mode of ice-filled cracks at different angles in Brazilian splitting test: (a)  $0^\circ$ , (b)  $30^\circ$ , (c)  $45^\circ$ , (d)  $60^\circ$ , (e)  $90^\circ$ .

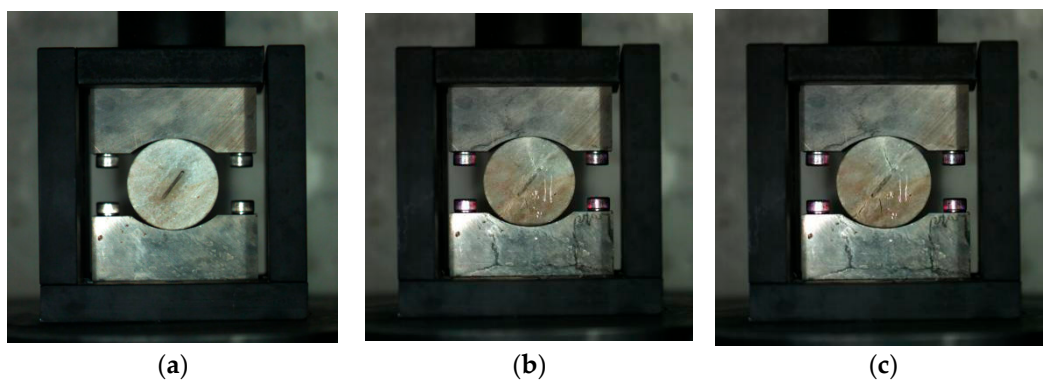


**Figure 7.** Fracture morphology process of a  $60^\circ$  ice-filled crack frozen rock specimen in Brazilian splitting test: (a) 0 s, (b) 90 s, (c) 100 s.

### 2.3. RFPA<sup>3D</sup> Feasibility Verification

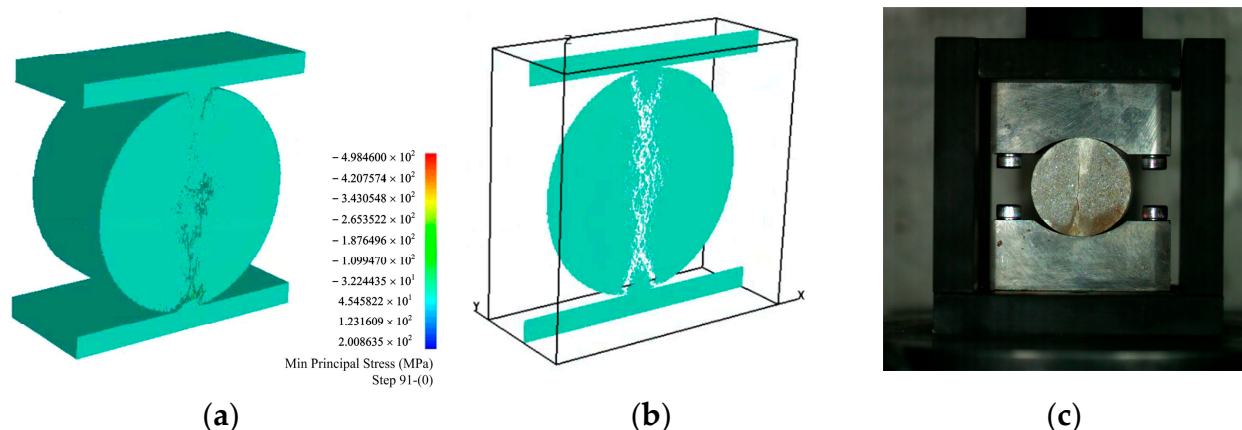
Rock is a heterogeneous material. The heterogeneity plays an important role in determining the crack initiation and fracture mode of rock mass. The influence of heterogeneity is pronounced in the progressive failure process. The Weibull distribution is used to consider the heterogeneity of rock in the RFPA method. RFPA is also suitable for the fracture analysis of brittle materials. Compared with ABAQUS and COMSOL, RFPA calculates crack initiation and propagation without considering the convergence problem. At present, a large number of papers have been published on numerical simulation analysis of rock materials using RFPA, and the principle can be found in the relevant papers [32–38].

RFPA<sup>3D</sup> was used to perform the splitting experiments of the frozen rock specimens. The aim of the simulation was to obtain the internal microcrack initiation and extension, and the energy accumulation and release in the process of frozen rock failure. The size of the model was  $\phi = 50 \times 25$  mm, and the mesh size was  $0.25 \times 0.5 \times 0.25$  mm. Cardboard was added at both ends to reduce the end effect. The thickness of the cardboard was 5 mm and the loading rate was 0.0005 mm/step. The material parameters of the model (Table 1) were obtained from the uniaxial compression of intact frozen rock and Brazilian splitting experiments, and converted by RFPA empirical formula [39,40].

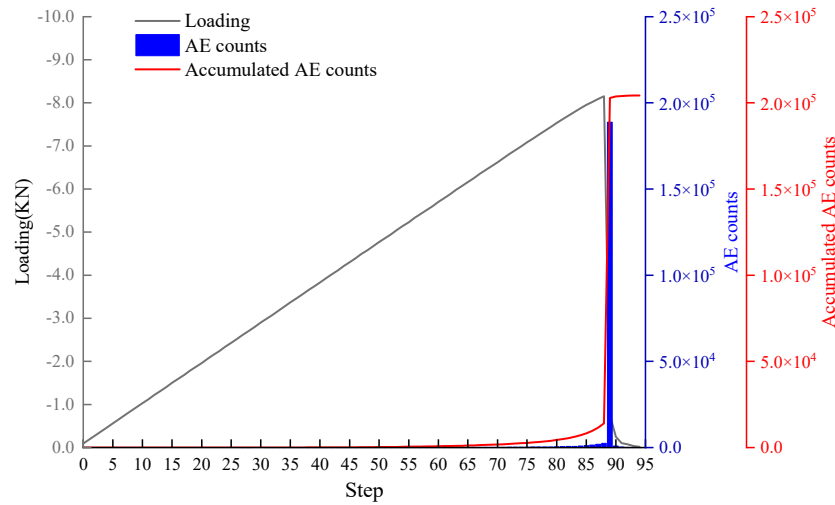
**Table 1.** Material parameters of the model.

|           | Elasticity Modulus (MPa) | m   | Compressive Strength (MPa) | m   | Poisson Ratio | Friction Angle |
|-----------|--------------------------|-----|----------------------------|-----|---------------|----------------|
| Granite   | 32,000                   | 5   | 147                        | 5   | 0.25          | 30°            |
| Ice       | 6000                     | 10  | 8                          | 10  | 0.35          | 26.5°          |
| Cardboard | 50,000                   | 100 | 1 e8                       | 100 | 0.3           | 30°            |

Figure 8 shows the numerical simulation results of the Brazilian splitting of intact frozen rock. Compared with the experimental results, the frozen rock fracture mode was similar, and macroscopic cracks were formed in the loading direction. The intact frozen rock specimen showed a typical brittle failure form. AE events increased sharply before macroscopic cracks occurred. The frozen rock specimen fractured instantly and released a large amount of energy (Figure 9). The load capacity of the intact frozen rock specimen was 8.15 kN in the numerical simulation and 8.88 kN in the experiment, which were similar to each other.

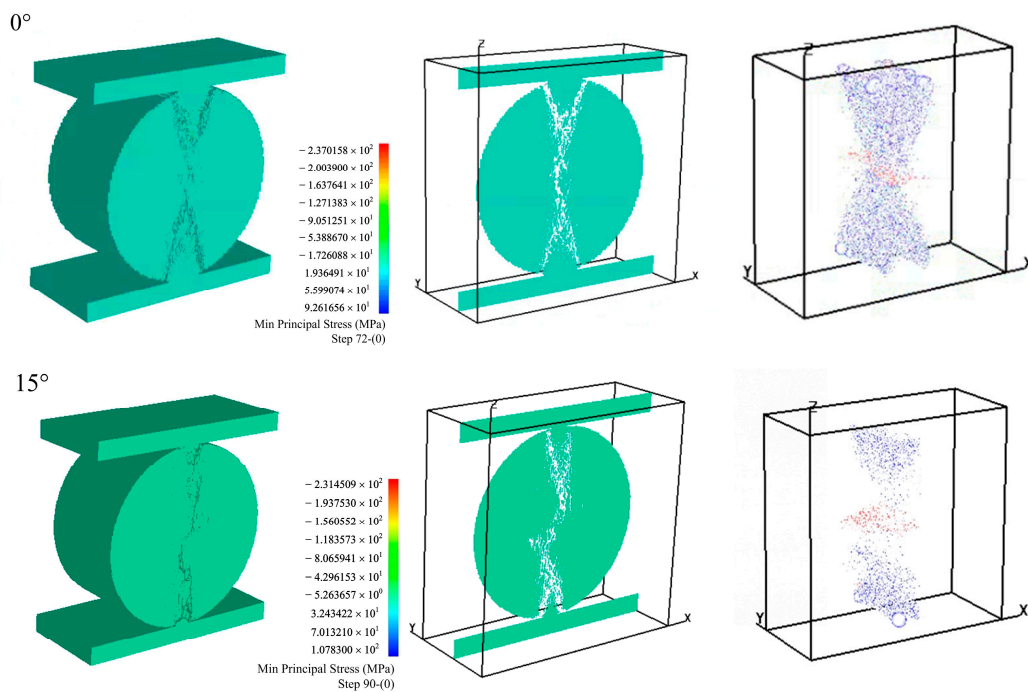


**Figure 8.** Numerical simulation results of Brazilian splitting of intact frozen rock: (a) minimum principal stress, (b) model slice, (c) fracture mode.



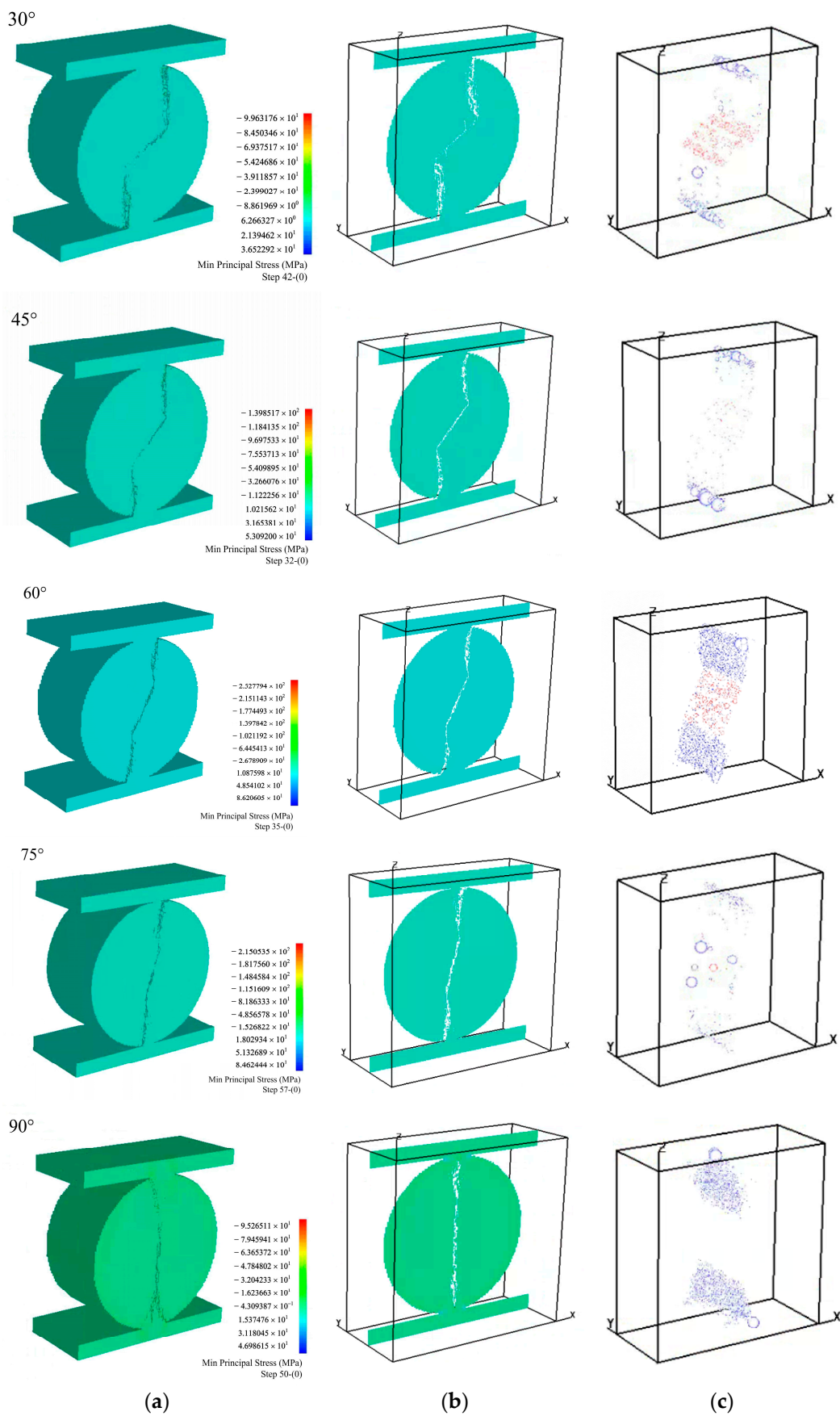
**Figure 9.** The relationship curve between load, AE counts and accumulated AE counts for intact frozen rock.

Figure 10 shows the numerical simulation results of the Brazilian splitting of frozen rock with different ice-filled crack angles. Red and blue circles in the AE distribution indicate the shear and tensile failure of the element. Compared with the experimental results (Figure 6), the splitting fracture modes of the frozen rock model were similar. The ice in the crack supported and transferred some force during the loading. However, the ice strength was lower than the rock strength, which induced the stress concentration at the ice-filled crack. When loaded to a certain extent, wing cracks occurred at the tip and penetrated through the whole model.



**Figure 10.** Cont.





**Figure 10.** Numerical simulation results of Brazilian splitting of frozen rock in different ice-filled crack angles: (a) minimum principal stress, (b) model slice; (c) AE.

Figure 11 shows the relationship curve between the load, AE counts and accumulated AE counts for frozen rock with different ice-filled crack angles. The peak load of 0° ice-filled crack frozen rock was 7.62 kN, and splitting failure occurred at step 67. The peak load of 15° ice-filled crack frozen rock was 6.81 kN, and splitting failure occurred in step 87. The peak load of 30° ice-filled crack frozen rock was 4.11 kN, and splitting failure occurred at step 38. The peak load of the 45° fractured frozen rock specimen was 2.59 kN, and splitting failure occurred in step 29.

The frozen rock specimens with 0°, 15°, 30°, and 45° ice-filled crack showed typical brittle failure mode. At the initial stage of loading, the internal microcracks of the frozen rock specimen accumulated continuously. AE events were fewer with no macroscopic cracks on the surface. When an ice-filled crack incurred damage and small macroscopic cracks began to appear on the surface of the specimen, AE events increased and the damaged elements accumulated stably. When the tensile strength increased to the peak value, the damaged elements increased. At the same time, the AE events increased suddenly, and the macroscopic cracks on the surface of the model further extended. When the stress fell, there were still a small number of AE events existing, and the damaged elements increased continuously. The cracks on the surface of the model were aggravated and extended, and the specimen finally failed.

The peak loads of the frozen rock with 60, 75 and 90° angle ice-filled cracks were 2.73, 2.57 and 3.49 kN, respectively, and the splitting failures occurred at steps 30, 38, and 34. There were two peak regions of AE events in these specimens. The first peak was the energy released by the ice-filled cracks, and the second peak was the brittle failure of the specimen. The frozen rock specimens with 60, 75 and 90° ice-filled cracks also showed a typical brittle failure mode.

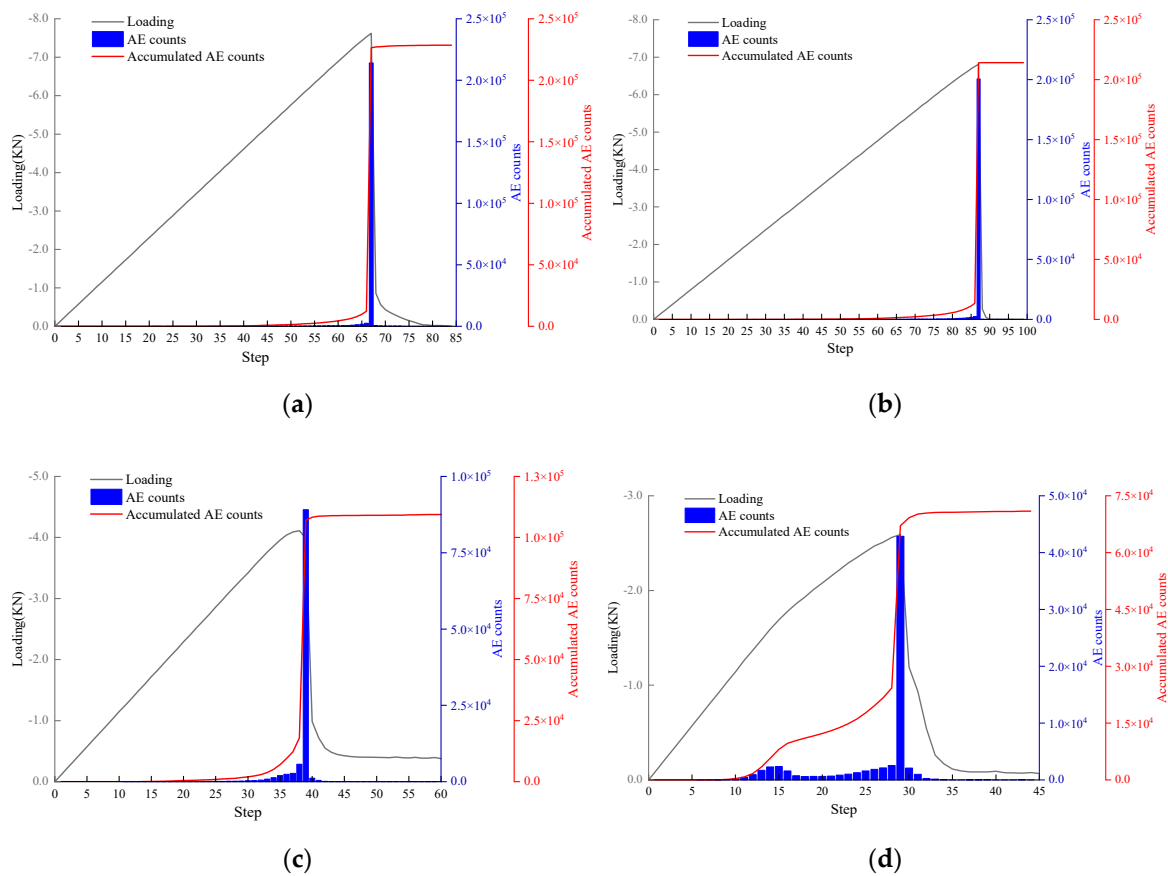
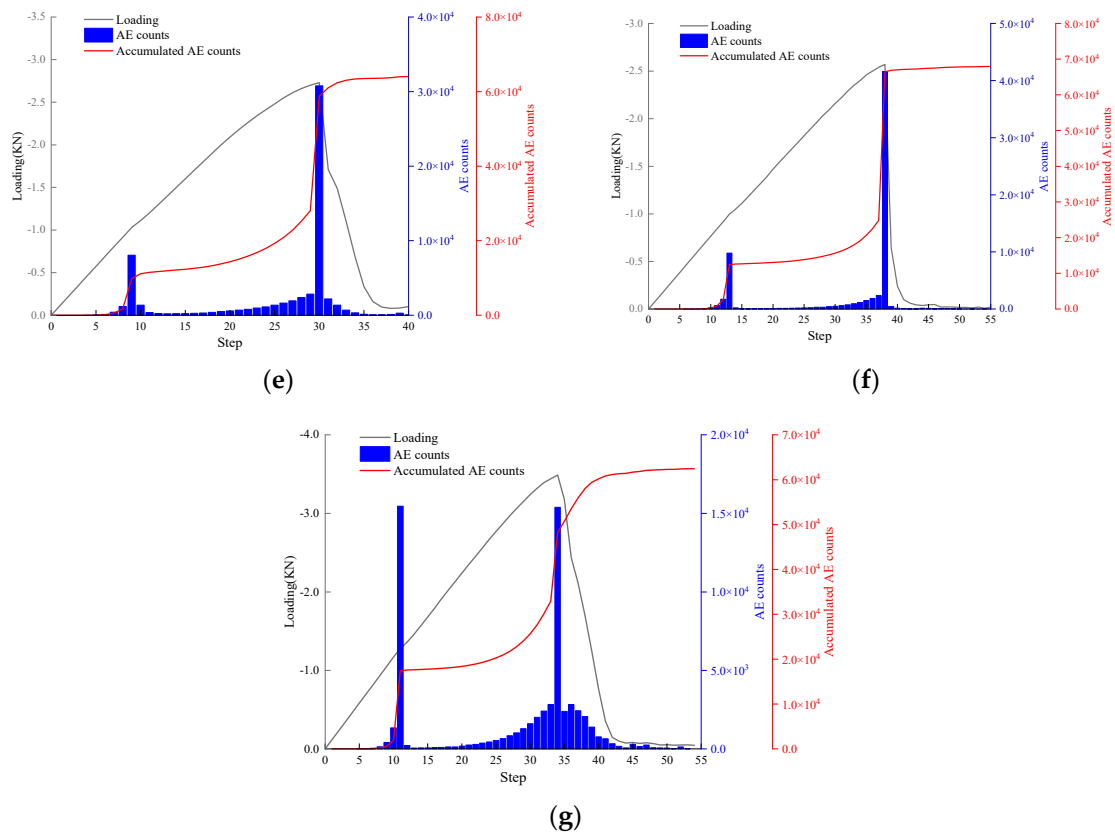
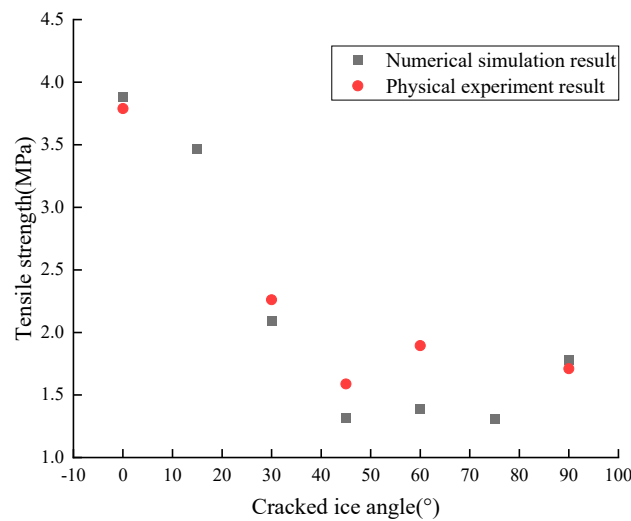


Figure 11. Cont.



**Figure 11.** The relationship curve between load, AE counts and accumulated AE counts for frozen rock with different ice-filled crack angles: (a) 0°, (b) 15°, (c) 30°, (d) 45°, (e) 60°, (f) 75°, (g) 90°.

Figure 12 shows that the numerical simulation results are close to the experimental results by comparing the tensile strength of frozen rock with different ice-filled angles. The tensile strength of the specimens decreased gradually and then increased with the increase in the angle of the ice-filled crack. By comparing the tensile strength and fracture mode of the frozen rock with the experimental results, it proves that RFPA<sup>3D</sup> is feasible for simulating the splitting process of frozen rock mass.



**Figure 12.** Comparison between experimental and simulated values of tensile strength of frozen rock.

### 3. Multi-Factor Discussion

In order to study the change of tensile strength, crack initiation and fracture mode of frozen rock under the influence of multiple factors, RFPA<sup>3D</sup> was used to conduct numerical simulation analysis on specimens with different widths of ice-filled crack ( $l = 20$  mm,  $\alpha = 60^\circ$ ,  $w = 2, 3, 4$  mm) and lengths of ice-filled crack ( $w = 1.5$  mm,  $\alpha = 30^\circ$ ,  $l = 10, 15, 25$  mm). The material parameters are shown in Table 1.

#### 3.1. Different Lengths for Ice-Filled Crack

Figure 13 shows that the fracture mode of the frozen rock specimens with different lengths of ice-filled crack started from the ice crack first, and then the wing crack was formed from the crack tip of the ice to the loading end.

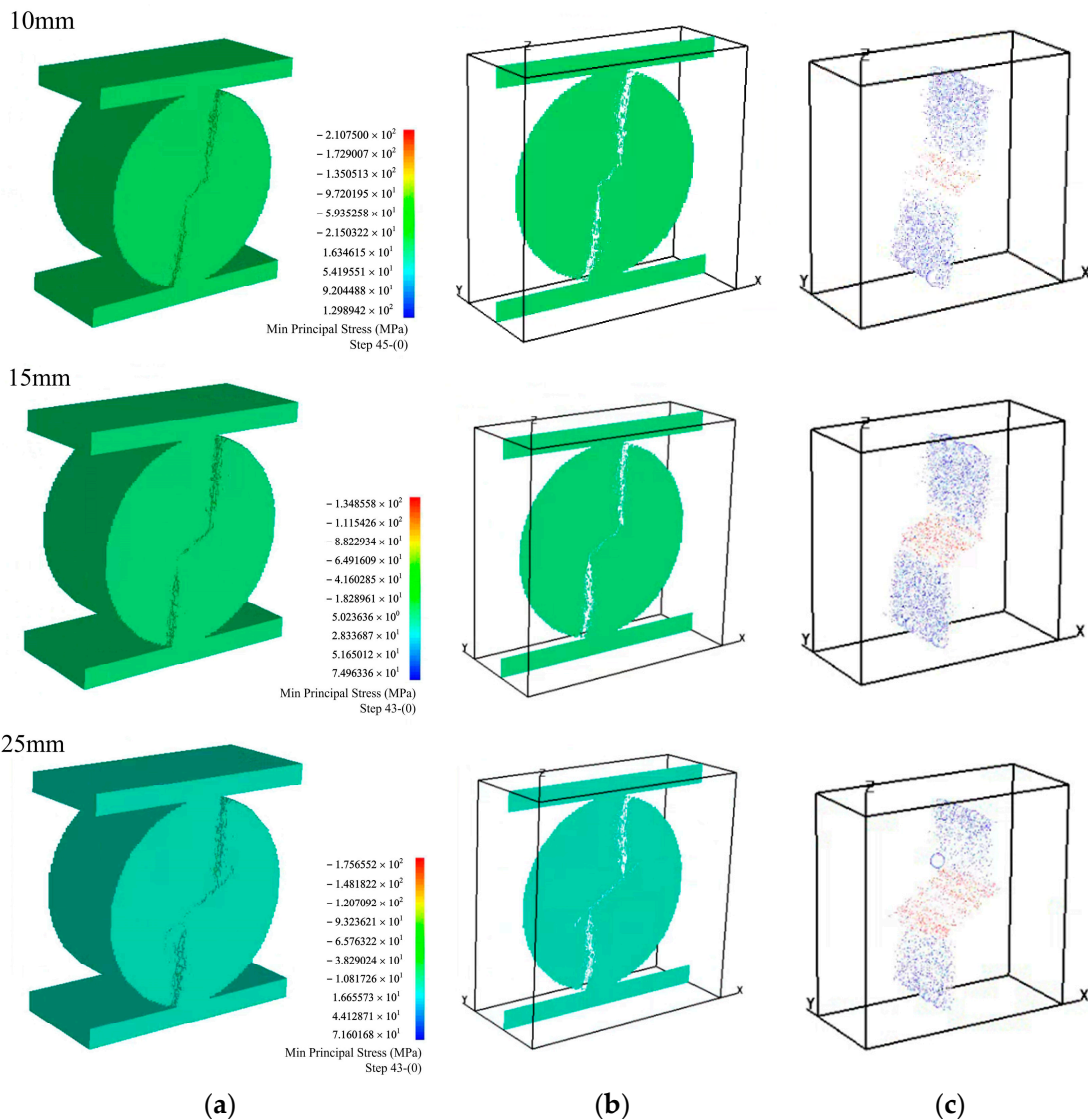


**Figure 13.** Brazilian splitting fracture mode of ice-filled crack frozen rock of different lengths. (a) Minimum principal stress, (b) model slice, (c) AE.

The peak loads of frozen rock with 10, 15, and 25 mm length ice-filled cracks were 4.63, 4.35, and 4.04 kN, respectively, and the splitting failure occurred at steps 42, 40, and 40 (Figure 14a–c). Combined with the calculation results for 20 mm length frozen fractured rock specimens in 2.3, it was found that the tensile strength of the frozen rock gradually decreased with the increase in the length of the ice-filled crack. The longer the ice-filled crack, the higher the ice content, and the lower the bearing capacity of the specimen.



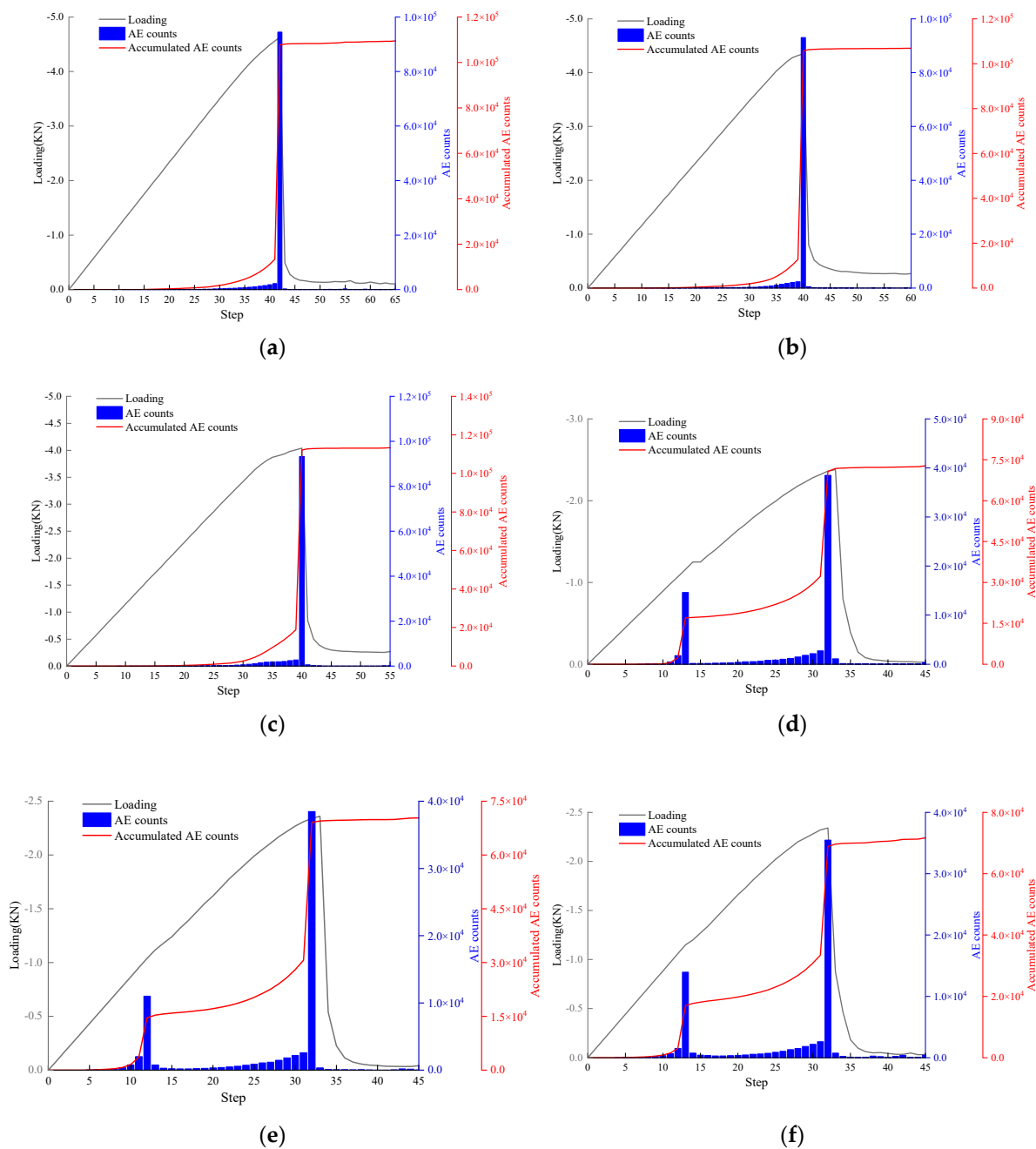


**Figure 14.** The relationship curve between load, AE counts and accumulated AE counts for ice-filled cracks of different lengths and widths of frozen rock. (a)  $l = 10$  mm, (b)  $l = 15$  mm, (c)  $l = 25$  mm, (d)  $w = 2$  mm, (e)  $w = 3$  mm, (f)  $w = 4$  mm.

### 3.2. Different Widths for Ice-Filled Cracks

Frozen rocks with different ice-filled crack widths also incur damage and failure elements from the ice. Then, the wing crack starts from the tip of the ice-filled crack, and gradually extends to the loading end (Figure 15). The peak loads of frozen rock with 2, 3, and 4 mm width ice-filled cracks were 2.38, 2.36, and 2.34 kN, respectively. Combined with the calculation results of 1.5 mm width frozen fractured rock specimens in 2.3, it was found that the tensile strength of frozen rock gradually decreased with the increase in the width of the ice-filled crack. There were also two peak regions of AE events (Figure 14d–e). The first peak was the energy released by the ice-filled crack, and the second peak was the brittle failure of the specimen.

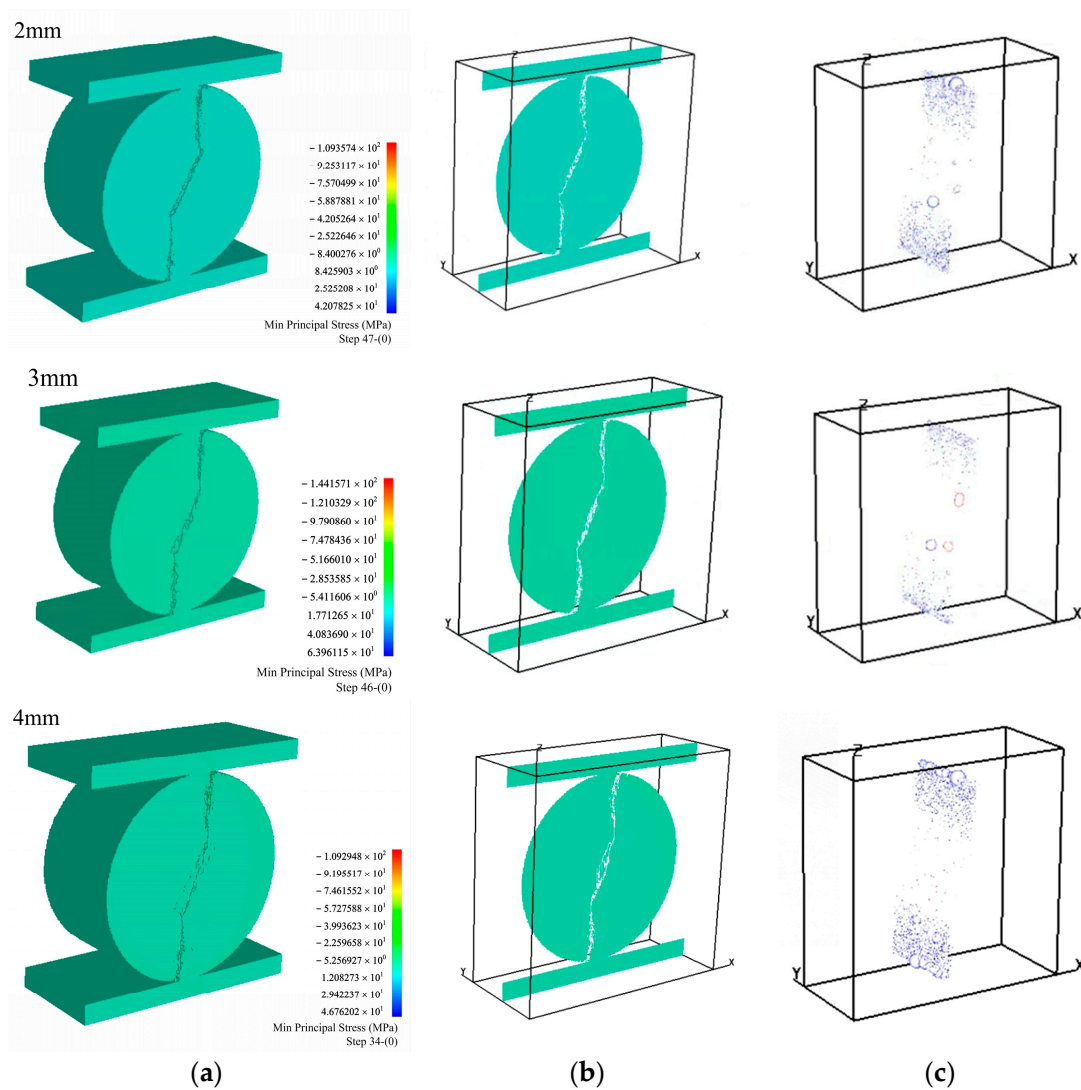


**Figure 15.** Brazilian splitting fracture mode of frozen rock with ice-filled cracks of different widths. (a) Minimum principal stress, (b) model slice, (c) AE.

#### 4. Conclusions

- (1). The tensile strength of frozen rock specimens decreased gradually and then increased with the increase in the ice-filled crack angle. When the ice-filled crack angle was  $0^\circ$ , the tensile strength of the ice-filled crack frozen rock specimen was similar to that of the intact frozen rock specimen. The tensile strength was the lowest when the ice-filled crack angle was  $45^\circ$ .
- (2). The peak loads of frozen rock with 1.5, 2, 3, and 4 mm width ice-filled cracks were 2.73, 2.38, 2.36, and 2.34 kN, respectively. The peak loads of frozen rock with 10, 15, 20, and 25 mm length ice-filled cracks were 4.63, 4.35, 4.11 and 4.04 kN, respectively. The tensile strength of frozen rock gradually decreased with the increase in the length and width of the ice-filled cracks.
- (3). Except for the  $0^\circ$  ice-filled cracks, the frozen fractured rock masses incurred damage elements at the ice-filled crack first, and then the wing crack started from the tip of the ice-filled crack and extended continuously, leading to the failure of the frozen rock specimens. When the angle of the ice-filled crack was  $0^\circ$ , the ice crack was perpendicular to the loading direction, and the effects on the frozen rock specimen were small.

- (4). The frozen rock specimens showed typical brittle failure characteristics. With the loading process, the model experienced four stages: internal microcrack initiation, surface macroscopic crack generation, macroscopic crack propagation, and complete failure.

**Author Contributions:** Conceptualization, T.W. and P.L.; methodology, T.W., C.T. and P.L.; software, T.W., J.Y. and C.T.; validation, T.W., T.G., J.Y. and B.Z.; formal analysis, T.W. and T.G.; investigation, T.W. and B.Z.; resources, T.W., C.T. and P.L.; data curation, T.W. and P.L.; writing—original draft preparation, T.W.; writing—review and editing, C.T. and P.L.; visualization, T.W.; supervision, C.T. and P.L.; project administration, C.T.; funding acquisition, C.T. and P.L. All authors have read and agreed to the published version of the manuscript.

**Funding:** This research was funded by the National Natural Science Foundation of China (Grant No. 42050201) and the Open Fund of State Key Laboratory of Frozen Soil Engineering (Grant No. SKLFSE202013).

**Institutional Review Board Statement:** Not applicable.

**Informed Consent Statement:** Informed consent was obtained from all subjects involved in the study.

**Data Availability Statement:** The data presented in this study are available on request from the corresponding author. The data are not publicly available due to privacy concerns.

**Acknowledgments:** Hongda Blasting Engineering Group Co., Ltd. are appreciated for their assistance.

**Conflicts of Interest:** The authors declare they have no conflict of interest to this work.

## References

- Huang, S.B.; Liu, Y.Z.; Guo, Y.L.; Zhang, Z.; Cai, Y. Strength and failure characteristics of rock-like material containing single crack under freeze-thaw and uniaxial compression. *Cold Reg. Sci. Technol.* **2019**, *162*, 1–10. [[CrossRef](#)]
- Liu, N.F.; Li, N.; Li, G.F.; Song, Z.P.; Wang, S.J. Method for Evaluating the Equivalent Thermal Conductivity of a Freezing Rock Mass Containing Systematic Fractures. *Rock Mech. Rock Eng.* **2022**, *55*, 7333–7355. [[CrossRef](#)]
- Wang, T.T.; Tang, C.A.; Li, P.F.; Tang, S.; Liu, M.H.; Zhang, B.B. Frost-Heaving Cracking Sensitivity of Single-Flaw Rock Mass Based on a Numerical Experimental Method. *Geofluids* **2021**, *2021*, 3436119. [[CrossRef](#)]
- Ma, D.D.; Xiang, H.S.; Ma, Q.Y.; Kaunda, E.E.; Huang, K.; Su, Q.Q.; Yao, Z.M. Dynamic damage constitutive model of frozen silty soil with prefabricated crack under uniaxial load. *J. Eng. Mech.* **2021**, *147*, 04021033. [[CrossRef](#)]
- Xu, S.H.; Li, N.; Wang, X.D.; Xu, Z.G.; Yuan, K.K.; Tian, Y.Z.; Wang, L.L. Damage test and degradation model of saturated sandstone due to cyclic freezing and thawing of rock slopes of open-pit coal mine. *Chin. J. Rock Mech. Eng.* **2016**, *35*, 2561–2571.
- Wu, N.; Liang, Z.Z.; Zhang, Z.H.; Li, S.H.; Lang, Y.X. Development and Verification of Three-Dimensional Equivalent Discrete Fracture Network Modelling Based on the Finite Element Method. *Eng. Geol.* **2022**, *306*, 106759. [[CrossRef](#)]
- Wan, W.; Li, C.C. Microscopic and Acoustic Interpretations of the Physics of Rock Burst and the Difference in Fracturing Patterns in Class I and Class II Rocks. *Rock Mech. Rock Eng.* **2022**, *55*, 6841–6862. [[CrossRef](#)]
- Yang, S.Q.; Yin, P.F.; Huang, Y.H. Experiment and Discrete Element Modelling on Strength, Deformation and Failure Behaviour of Shale under Brazilian Compression. *Rock Mech. Rock Eng.* **2019**, *52*, 4339–4359. [[CrossRef](#)]
- Wang, M.; Ping, C. Experimental study on the validity and rationality of four Brazilian disc tests. *Geothch. Geol. Eng.* **2018**, *36*, 63–76. [[CrossRef](#)]
- Haeri, H.; Shahriar, K.; Marji, M.F.; Moarefvand, P. Experimental and numerical study of crack propagation and coalescence in pre-cracked rock-like disks. *Int. J. Rock Mech. Min. Sci.* **2014**, *67*, 20–28. [[CrossRef](#)]
- Gao, M.; Liang, Z.Z.; Jia, S.P.; Zou, J.Q. Tensile Properties and Tensile Failure Criteria of Layered Rocks. *Appl. Sci.* **2022**, *12*, 6063. [[CrossRef](#)]
- Zhou, J.; Zeng, Y.J.; Guo, Y.T.; Chang, X.; Liu, L.W.; Wang, L.; Hou, Z.K.; Yang, C.H. Effect of natural filling fracture on the cracking process of shale Brazilian disc containing a central straight notched flaw. *J. Pet. Sci. Eng.* **2021**, *196*, 107993. [[CrossRef](#)]
- Zhao, Z.H.; Liu, Z.N.; Pu, H.; Li, X. Effect of thermal treatment on Brazilian tensile strength of granites with different grain size distributions. *Rock Mech. Rock Eng.* **2018**, *51*, 1293–1303. [[CrossRef](#)]
- Liu, B.; Sun, Y.D.; Wang, B.; Han, Y.H.; Zhang, R.H.; Wang, J.X. Effect of water content on mechanical and electrical characteristics of the water-rich sandstone during freezing. *Environ. Earth Sci.* **2020**, *79*, 236–249. [[CrossRef](#)]
- Jia, H.L.; Zi, F.; Yang, G.S.; Li, G.Y.; Shen, Y.J.; Sun, Q.; Yang, P.Y. Influence of pore water (ice) content on the strength and deformability of frozen argillaceous siltstone. *Rock Mech. Rock Eng.* **2020**, *53*, 967–974. [[CrossRef](#)]
- Kodama, J.; Goto, T.; Fujii, Y.; Hagan, P. The effects of water content, temperature and loading rate on strength and failure process of frozen rocks. *Int. J. Rock Mech. Min. Sci.* **2013**, *62*, 1–13. [[CrossRef](#)]
- Wang, Y.; Yi, Y.F.; Li, C.H.; Han, J.Q. Anisotropic fracture and energy characteristics of a Tibet marble exposed to multi-level constant-amplitude (MLCA) cyclic loads: A lab-scale testing. *Eng. Fract. Mech.* **2021**, *244*, 107550. [[CrossRef](#)]

18. Jia, H.L.; Ding, S.; Zi, F.; Dong, Y.H.; Shen, Y.J. Evolution in sandstone pore structures with freeze-thaw cycling and interpretation of damage mechanisms in saturated porous rocks. *Catena* **2020**, *195*, 104915. [[CrossRef](#)]
19. Zhou, X.P.; Fu, Y.H.; Wang, Y.; Zhou, J.N. Experimental study on the fracture and fatigue behaviors of flawed sandstone under coupled freeze-thaw and cyclic loads. *Theor. Appl. Fract. Mech.* **2022**, *119*, 103299. [[CrossRef](#)]
20. Zhang, H.M.; Xia, H.J.; Yang, G.S.; Zhang, M.J.; Peng, C.; Ye, W.J.; Shen, Y.J. Experimental research of influences of freeze-thaw cycles and confining pressure on physical-mechanical characteristics of rocks. *J. China Coal Soc.* **2018**, *43*, 441–448.
21. Bayram, F. Predicting mechanical strength loss of natural stones after freeze-thaw in cold regions. *Cold Reg. Sci. Technol.* **2012**, *83–84*, 98–102. [[CrossRef](#)]
22. Aoki, K.; Hibiya, K.; Yoshida, T. Storage of refrigerated liquefied gases in rock caverns: Characteristics of rock under very low temperatures. *Tunn. Undergr. Space Technol.* **1990**, *5*, 319–325. [[CrossRef](#)]
23. Yamabe, T.; Neaupane, K.M. Determination of some thermo-mechanical properties of Sirahama sandstone under subzero temperature conditions. *Int. J. Rock Mech. Min. Sci.* **2001**, *38*, 102–1034. [[CrossRef](#)]
24. Xu, G.M.; Liu, Q.S.; Peng, W.W.; Chang, X.X. Experimental study on basic mechanical behaviors of rocks under low temperatures. *Chin. J. Rock Mech. Eng.* **2006**, *25*, 2502–2508. (In Chinese)
25. Yang, G.S.; Xi, J.M.; Li, H.J.; Cheng, L. Experimental study of rock mechanical properties under triaxial compressive and frozen conditions. *Chin. J. Rock Mech. Eng.* **2010**, *29*, 459–464. (In Chinese)
26. Xi, J.M.; Yang, G.S.; Pang, L.; Lv, X.T.; Liu, F.L. Experimental study on basic mechanical behaviors of sandy mudstone under low freezing temperature. *J. China Coal Soc.* **2014**, *39*, 1262–1268.
27. Shan, R.L.; Yang, H.; Guo, Z.M.; Liu, X.; Song, L. Experimental study of strength characters of saturated red sandstone on negative temperature under triaxial compression. *Chin. J. Rock Mech. Eng.* **2014**, *33*, 3657–3664.
28. Li, T.; Ma, Y.J.; Liu, B.; Sheng, H.L.; He, P. Strength characteristics and elastic modulus evolution of frozen gray sandstone under cyclic loading. *J. China Coal Soc.* **2018**, *43*, 2438–2443.
29. Bai, Y.; Shan, R.L.; Ju, Y.; Wu, Y.X.; Tong, X.; Han, T.Y.; Dou, H.Y. Experimental study on the strength, deformation and crack evolution behaviour of red sandstone samples containing two ice-filled fissures under triaxial compression. *Cold Reg. Sci. Technol.* **2020**, *174*, 103061. [[CrossRef](#)]
30. Yang, H.; Shan, R.L.; Zhang, J.X.; Wu, F.M.; Guo, Z.M. Mechanical properties of frozen rock mass with two diagonal intersected fractures. *Int. J. Min. Sci. Technol.* **2018**, *28*, 631–638. [[CrossRef](#)]
31. Shloido, G.A. Determining the tensile strength of frozen ground. *Hydrotech. Constr.* **1968**, *2*, 238–240. [[CrossRef](#)]
32. Wang, S.Y.; Sloan, S.W.; Tang, C.A. Three-dimensional numerical investigations of the failure mechanism of a rock disc with a central or eccentric hole. *Rock Mech. Rock Eng.* **2014**, *47*, 2117–2137. [[CrossRef](#)]
33. Fan, N.; Wang, J.R.; Deng, C.B.; Fan, Y.P.; Wang, T.T.; Guo, X.Y. Quantitative Characterization of Coal Microstructure and Visualization Seepage of Macropores Using CT-Based 3D Reconstruction. *J. Nat. Gas Sci. Eng.* **2020**, *81*, 103384. [[CrossRef](#)]
34. Liang, Z.; Wu, N.; Li, Y.; Li, H.; Li, W. Numerical Study on Anisotropy of the Representative Elementary Volume of Strength and Deformability of Jointed Rock Masses. *Rock Mech. Rock Eng.* **2019**, *52*, 4387–4402. [[CrossRef](#)]
35. Khoojine, A.S.; Shadabfar, M.; Tabriz, Y.E. A Mutual Information-Based Network Autoregressive Model for Crude Oil Price Forecasting Using Open-High-Low-Close Prices. *Mathematics* **2022**, *10*, 10173172.
36. Zhu, W.C.; Tang, C.A. Numerical simulation of Brazilian disk rock failure under static and dynamic loading. *Int. J. Rock Mech. Min. Sci.* **2006**, *43*, 236–252. [[CrossRef](#)]
37. Wu, N.; Liang, Z.Z.; Li, Y.; Qian, X.K.; Gong, B. Effect of confining stress on representative elementary volume of jointed rock masses. *Geomech. Eng.* **2019**, *18*, 627–638.
38. Shadabfar, M.; Cheng, L.S. Probabilistic Approach for Optimal Portfolio Selection Using a Hybrid Monte Carlo Simulation and Markowitz Model. *Alex. Eng. J.* **2020**, *59*, 3381–3393. [[CrossRef](#)]
39. Tang, C.A. Numerical simulation of progressive rock failure and associated seismicity. *Int. J. Rock Mech. Min. Sci.* **1997**, *34*, 249–261. [[CrossRef](#)]
40. Liao, Z.Y.; Zhu, J.B.; Tang, C.A. Numerical investigation of rock tensile strength determined by direct tension, Brazilian and three-point bending tests. *Int. J. Rock Mech. Min. Sci.* **2019**, *115*, 21–32. [[CrossRef](#)]